

LONG-LIVED PROTOPLANETARY DISKS IN MULTIPLE SYSTEMS: THE VLA VIEW OF HD 98800

ÁLVARO RIBAS¹, ENRIQUE MACÍAS¹, CATHERINE C. ESPAILLAT¹, GASPARD DUCHÊNE^{2,3}

¹Department of Astronomy, Boston University, Boston, MA 02215, USA; aribas@bu.edu

²Department of Astronomy, UC Berkeley, Berkeley, CA 94720, USA

³Univ. Grenoble Alpes/CNRS, IPAG, F-38000 Grenoble, France

ABSTRACT

The conditions and evolution of protoplanetary disks in multiple systems can be considerably different from those around single stars, which may have important consequences for planet formation. We present Very Large Array (VLA) 8.8 mm (34 GHz) and 5 cm (6 GHz) observations of the quadruple system HD 98800, which consists of two spectroscopic binary systems (Aa-Ab, Ba-Bb). The Ba-Bb pair is surrounded by a circumbinary disk, which is usually assumed to be a debris disk given its ~ 10 Myr age and the lack of near infrared excess. The VLA 8.8 mm observations resolve the disk size (5-5.5 au) and its inner cavity (≈ 3 au) for the first time, making it one of the smallest disks known. Its small size, large fractional luminosity, and millimeter spectral index consistent with blackbody emission support the idea that HD 98800 B is a massive, optically thick ring that may still retain significant amounts of gas. The disk detection at 5 cm is compatible with free-free emission from photoionized material. The diskless HD 98800 A component is also detected, showing partial polarization at 5 cm that is compatible with nonthermal chromospheric activity. We propose that tidal torques from Ba-Bb and A-B have stopped the viscous evolution of the inner and outer disk radii, and the disk is evolving via mass loss through photoevaporative winds. This scenario can explain the properties and longevity of HD 98800 B as well as the lack of a disk around HD 98800 A, suggesting that planet formation could have more time to proceed in multiple systems than around single stars in certain system configurations.

Keywords: binaries: general — protoplanetary disks — stars: individual (HD 98800) — stars: pre-main sequence — techniques: interferometric

1. INTRODUCTION

Given the abundance of binaries and multiple systems in our Galaxy, understanding planet formation in these systems represents an important piece of our knowledge of exoplanetary populations. In fact, 30-75% of stars appear to have formed in multiple systems (Duquennoy & Mayor 1991; Kraus et al. 2008; Lafrenière et al. 2008; Kraus et al. 2011; Duchêne & Kraus 2013), and various exoplanets have already been found around binary and multiple systems (e.g. Doyle et al. 2011; Welsh et al. 2012; Dupuy et al. 2016; Kostov et al. 2016).

The formation of planets around single stars occurs in the protoplanetary disks surrounding young stars. These disks contain gas and dust which, via dust growth first and gas accretion later, can form rocky and gas giant planets (Raymond et al. 2014; Helled et al. 2014; Testi et al. 2014). At the same time, processes such as the viscous evolution of the disk (e.g. Shakura & Sunyaev 1973; Lynden-Bell & Pringle 1974; Hartmann et al. 1998), photoevaporation by stellar radiation (e.g. Shu et al. 1993; Hollenbach et al. 1994), or the interaction

with newborn planets (Kley & Nelson 2012; Espaillat et al. 2014) lead to the eventual dispersal of the disk (see Alexander et al. 2014, and references therein), which occurs 5-10 Myr after their formation (Haisch et al. 2001; Hernández et al. 2007, 2008; Mamajek 2009; Ribas et al. 2015). Once the protoplanetary disk disperses, a second generation of dust produced by planetesimal collisions (with some possible contribution from remaining dust from the protoplanetary phase) forms a gas-poor, less massive, colder disk called a debris disk, analogous to our own Kuiper Belt (e.g. Wyatt 2008; Hughes et al. 2018). While the latter can survive for much longer (\sim Gyr) thanks to dust replenishment from these collisions, the transition from a protoplanetary to a debris disk is still not well understood. The importance of disk evolution and dispersal is obvious, since it sets a time limit to planet formation and determines many of the properties of the resulting planetary systems.

This scenario can change significantly in binary or multiple systems; the gravitational interaction of a (sub)stellar companion can have an important effect on

disks, leading to truncation or even quick dispersal depending on various parameters, such as the semi-major axis of the binary orbit, its eccentricity, or the masses of the components (e.g. [Papaloizou & Pringle 1977](#); [Artymowicz & Lubow 1994](#)). In fact, various surveys have shown the fraction of protoplanetary disks to be smaller around close ($a < 40$ au) binaries than around single stars or wide binaries ([Cieza et al. 2009](#); [Harris et al. 2012](#); [Kraus et al. 2012](#)). On the other hand, very close binaries (a few au) may not be able to retain individual circumstellar disks (disks around individual components of the system), but could harbor a circumbinary disk surrounding both stars. Mass accretion rates in circumbinary disks can be severely diminished due to the tidal torques exerted by the central sources, resulting in extended disk lifetimes (e.g. [Alexander 2012](#)). Also, disks with truncated outer radii due to a close companion may even experience an outside-in evolution ([Rosotti & Clarke 2018](#)), which is completely different from the expectation for disks around single stars. All these mechanisms are likely to result in different populations of exoplanets around binary and multiple stars and are thus key pieces for understanding them.

In this study, we present NSF’s Karl G. Jansky Very Large Array (VLA) observations of an extreme case of a circumstellar disk in a multiple system: the hierarchical quadruple system HD 98800. The VLA observations resolved both the size and the inner cavity of the disk around HD 98800 B for the first time and shed light onto the puzzling existence of long-lived disks in multiple systems. The paper is outlined as follows: Sec. 2 provides a description of the HD 98800 system. Sec. 3 describes the VLA observations and ancillary data used, and the results and modeling procedure are discussed in Sec. 4. In Sec. 5, we examine the nature of the disk around HD 98800 B, compare our results with previous studies, and discuss implications for disks in multiple systems. Finally, our conclusions are presented in Sec. 6.

2. THE HD 98800 SYSTEM

HD 98800 is a hierarchical quadruple system located in the 7-10 Myr old TW Hya association ([Soderblom et al. 1996](#); [Webb et al. 1999](#); [Prato et al. 2001](#); [Torres et al. 2008](#); [Ducourant et al. 2014](#)). It was first identified as a possible T Tauri star by [Gregorio-Hetem et al. \(1992\)](#), together with other members of TW Hya. At ≈ 45 pc ([van Leeuwen 2007](#)), this source comprises two spectroscopic binary systems (A and B) orbiting each other with a semi-major axis of ≈ 45 au ($P = 214$ years, [Tokovinin et al. 2014](#)). While the orbital parameters of the southern component (Aa-Ab) are uncertain, [Boden et al. \(2005\)](#) used interferometric data to measure the orbits of the northern one (Ba-Bb) and found two stars of comparable masses ($M_{Ba} = 0.7 M_{\odot}$, $M_{Bb} = 0.6 M_{\odot}$)

Table 1. Properties of HD 98800.

Parameter	Value	Reference
Distance	45 pc	1
Age	7-10 Myr	2
A Component (Aa+Ab)		
a_{A-B}	45 au	3
e_{A-B}	0.4	3
i_{A-B}	88°	3
$M_A(Aa+Ab)^{\dagger}$	$1.3 M_{\odot}$	4
A_v	0 mag	5
B Component		
a_{Ba-Bb}	0.5 au	6
e_{Ba-Bb}	0.78	6
i_{Ba-Bb}	67°	6
M_{Ba}	$0.7 M_{\odot}$	6
M_{Bb}	$0.6 M_{\odot}$	6
$T_{\text{eff},Ba}$	4200 K	6
$T_{\text{eff},Bb}$	4000 K	6
$R_{\text{eff},Ba}$	$1.1 R_{\odot}$	6
$R_{\text{eff},Bb}$	$0.9 R_{\odot}$	6
A_v	0.44 mag	7

\dagger : uncertain

References. (1) [van Leeuwen \(2007\)](#), (2) [Ducourant et al. \(2014\)](#), (see the text for additional references), (3) [Tokovinin et al. \(2014\)](#), (4) [Tokovinin \(1999\)](#), (5) [Koerner et al. \(2000\)](#), (6) [Boden et al. \(2005\)](#), (7) [Soderblom et al. \(1998\)](#).

orbiting with a semi-major axis of $a \approx 0.5$ au ($P = 315$ days) and a high eccentricity ($e = 0.78$). The orbital period of Aa-Ab is believed to be similar ([Torres et al. 1995](#)). The relevant properties of HD 98800 adopted in the paper are listed in Table. 1.

The presence of circumstellar material was revealed by the conspicuous infrared (IR) excess in the system ([Walker & Wolstencroft 1988](#); [Zuckerman & Becklin 1993](#)) and was later attributed to the B component alone using high-resolution observations (e.g. [Koerner et al. 2000](#); [Prato et al. 2001](#)). The lack of emission at near-IR wavelengths, together with modeling of both the Spectral Energy Distribution (SED) and architecture of the system, suggested the existence of a small (a few au) cavity in the disk and a severely truncated outer radius (e.g. [Prato et al. 2001](#); [Akeson et al. 2007](#); [Pichardo et al. 2008](#)), as expected by the effect of the Ba-Bb and A-B pairs, respectively (e.g. [Artymowicz & Lubow 1994](#)). The dust composition was first studied in detail by [Furlan et al. \(2007\)](#), who presented the *Spitzer*/Infrared Spectrograph (IRS) of the source and found a broad silicate feature, indicating the presence of large grains. They proposed that some optically thin

dust is required inside the disk cavity ($\approx 1.5 - 2$ au) to account for the observed mid-IR spectrum, and reproduced the continuum emission with an optically thick ring at ≈ 6 au. Later, [Olofsson et al. \(2012\)](#) suggested that a small fraction of crystalline grains exist in the disk. The disk was finally (partially) resolved at $880 \mu\text{m}$ by [Andrews et al. \(2010\)](#) using the Submillimeter Array (SMA) interferometer, finding a disk extent of 10-15 au. They did not detect CO(3-2) emission from the system.

The disk around HD 98800 B is peculiar; due to its age, lack of signatures of mass accretion or molecular gas ([Soderblom et al. 1996](#); [Kastner et al. 2004](#); [Dent et al. 2005](#); [Salyk et al. 2009](#)), and deficit of near-IR excess, the object has usually been classified as an unusual debris disk ([Verrier & Evans 2008](#); [Olofsson et al. 2012](#)). On the other hand, later detections of H_2 ([Yang et al. 2012](#)) and [O I] ([Riviere-Marichalar et al. 2013](#)), together with its strong excess in the far-IR with respect to typical the debris disk (e.g. [Kennedy & Wyatt 2012](#)) also suggest that the object could be in a transitional phase from protoplanetary to a debris disk (e.g. [Wyatt et al. 2007](#)). Given the typical lifetimes of protoplanetary disks around single stars, the survival of a disk such as the one in HD 98800 B in a multiple system (subject to strong dynamical interactions) has been challenging for disk evolution theories.

3. OBSERVATIONS

3.1. VLA observations

We present resolved Ka band (≈ 9 mm) and C band (≈ 5 cm) data of HD 98800 obtained with the VLA of the National Radio Astronomy Observatory (NRAO)¹ within the Disks@EVLA program (Project code: AC982, P.I.: Claire Chandler). Both sets of observations were performed with the A configuration, which provides the longest baselines (from 0.7 to 36.4 km).

The Ka band observations were carried out on 2012 October 27 and 28, with a total on-source time of 169 minutes. A total bandwidth of 2 GHz was used, covering the frequency ranges from 30 to 31 GHz and from 37 to 38 GHz. The C band data were obtained on 2011 July 6, with the correlator set up to cover the frequencies from ≈ 4.3 GHz to ≈ 5.3 GHz and from ≈ 6.8 to ~ 7.8 GHz, resulting in a total bandwidth of 2 GHz. The on-source time for the C band was 20.5 minutes. At both bands, 3C286 was observed to perform the absolute flux calibration, while J1112-2158 was used to obtain the gain calibration. Additionally, 3C279 was used as the bandpass calibrator during the Ka band observa-

tions.

3.2. Spectral Energy Distribution (SED) compilation

To complement the VLA observations, we compiled photometry for both the A and B components from several studies, including [Rucinski \(1993\)](#), [Zuckerman & Becklin \(1993\)](#), [Sylvester et al. \(1996\)](#), [Soderblom et al. \(1998\)](#), [Low et al. \(1999\)](#), [Koerner et al. \(2000\)](#), [Prato et al. \(2001\)](#), [Di Francesco et al. \(2008\)](#), and [Andrews et al. \(2010\)](#). We also included data from the AKARI/IRC ([Ishihara et al. 2010](#)) and AKARI/FIS catalogs. Most of the emission at wavelengths $\geq 6 \mu\text{m}$ arises from the disk around HD 98800 B ([Furlan et al. 2007](#)); therefore, we assigned all data at wavelengths longer than this value to the B component. The photometry of HD 98800 B was then dereddened using the [Mathis \(1990\)](#) extinction law and $A_V = 0.44$ ([Soderblom et al. 1998](#)). We also included the *Spitzer*/IRS spectrum (corrected from the contribution of the A component) presented in [Furlan et al. \(2007\)](#).

Table 2. Photometry of HD 98800 A

Wavelength (μm)	Flux (mJy)	Reference
(1)	(2)	(3)
0.429	266 \pm 8	1
0.525	700 \pm 20	1
0.954	2080 \pm 60	1
0.955	2000 \pm 60	1
1.082	2440 \pm 80	1
1.251	2000 \pm 200	2
1.452	2470 \pm 70	1
1.658	2300 \pm 200	2
1.875	2190 \pm 70	1
1.899	2300 \pm 70	1
2.20	1800 \pm 100	2
4.7	470 \pm 40	3
4.8	450 \pm 50	2
7.9	180 \pm 30	2
7.91	180 \pm 20	4
8.80	200 \pm 20	2
8.81	170 \pm 10	4
9.69	150 \pm 20	4
9.80	160 \pm 10	2
10.3	120 \pm 10	4
10.3	140 \pm 10	2
11.7	140 \pm 10	2
11.7	100 \pm 10	4

Table 2 continued

¹ The NRAO is a facility of the National Science Foundation operated under cooperative agreement by Associated Universities, Inc.

Table 2 (*continued*)

Wavelength (μm)	Flux (mJy)	Reference
(1)	(2)	(3)
12.5	80 \pm 10	4
12.5	140 \pm 20	2
18.2	80 \pm 30	2
8820	0.080 \pm 0.015	This work
49600	0.16 \pm 0.03	This work

NOTE—**References.** (1) [Soderblom et al. \(1998\)](#), (2) [Prato et al. \(2001\)](#), (3) [Zuckerman & Becklin \(1993\)](#), (4) [Koerner et al. \(2000\)](#).

Additionally, the *Herschel Space Observatory* ([Pilbratt et al. 2010](#)) observed HD 98800 with both the Photocouductor Array Camera and Spectrometer (PACS) and the Spectral and Photometric Imaging Receiver (SPIRE) instruments. For PACS, observations at 70 μm (obsid: 1342188473), 100, and 160 μm (obsids: 1342212634 and 1342212635) are available (P.I.: B. Dent). We used the *Herschel* Interactive Processing Environment (HIPE v.15, [Ott 2010](#)) to perform aperture photometry using standard values: aperture radii of 12, 12, and 22 arcsec for 70, 100, and 160 μm , respectively; background annulus radii of 35 and 45 arcsec for all bands; and the corresponding aperture corrections ([Balog et al. 2014](#)). For SPIRE, observations at 250, 350, and 500 μm (obsid: 1342247269, P.I.: A. Roberge) were used to estimate photometric fluxes using the recommended procedure of fitting the sources in the timeline ([Pearson et al. 2014](#)). The *Herschel* fluxes were attributed to HD 98800 B. We note that the PACS fluxes listed in this study are 5-20% higher than the ones reported in [Riviere-Marichalar et al. \(2013\)](#), which is likely a result of the updated HIPE version and aperture correction factors used.

The photometry for the A and B components is presented in Tables 2 and 3, respectively.

Table 3. Photometry of HD 98800 B

Wavelength (μm)	Flux (mJy)	Reference
(1)	(2)	(3)
0.429	125 \pm 4	1
0.525	430 \pm 13	1
0.954	1880 \pm 60	1

Table 3 continued

Table 3 (*continued*)

Wavelength (μm)	Flux (mJy)	Reference
(1)	(2)	(3)
0.955	1890 \pm 60	1
1.082	2300 \pm 70	1
1.251	2200 \pm 200	2
1.658	2500 \pm 200	2
2.20	1790 \pm 100	2
4.68	720 \pm 40	3
4.80	580 \pm 60	2
7.90	430 \pm 50	2
7.91	440 \pm 20	2
8.80	890 \pm 50	2
8.81	830 \pm 30	4
9	1100 \pm 30	5
9.69	1620 \pm 70	4
9.80	1470 \pm 80	2
10.3	1900 \pm 80	4
10.3	1610 \pm 90	2
11.7	2030 \pm 110	2
11.7	2180 \pm 90	4
12.5	2020 \pm 80	4
12.5	2200 \pm 120	2
17.9	5000 \pm 300	4
18	6200 \pm 200	5
18.2	4900 \pm 500	2
20.8	5500 \pm 300	4
23.4	8500 \pm 400	6
24.5	8600 \pm 400	4
25	9700 \pm 800	7
60	7100 \pm 700	7
65	7000 \pm 2000	AKARI/FIS
70	7500 \pm 400	This work
71	6300 \pm 1200	6
90	5800 \pm 1300	AKARI/FIS
100	4300 \pm 300	7
100	4600 \pm 200	This work
156	2100 \pm 400	6
160	2500 \pm 100	This work
250	1120 \pm 40	This work
350	600 \pm 20	This work
450	500 \pm 200	8
500	310 \pm 12	This work
800	100 \pm 10	9

Table 3 continued

Table 3 (*continued*)

Wavelength (μm)	Flux (mJy)	Reference
(1)	(2)	(3)
850	70 ± 20	8
880	83 ± 3	10
1100	63 ± 6	11
1300	36 ± 7	12
2000	25 ± 3	11
8824	0.81 ± 0.09	This work
49600	0.09 ± 0.03	This work

NOTE—**References.** (1) [Soderblom et al. \(1998\)](#), (2) [Prato et al. \(2001\)](#), (3) [Zuckerman & Becklin \(1993\)](#), (4) [Koerner et al. \(2000\)](#), (5) [Ishihara et al. \(2010\)](#), (6) [Low et al. \(2005\)](#), (7) [Low et al. \(1999\)](#), (8) [Di Francesco et al. \(2008\)](#), (9) [Rucinski \(1993\)](#), (10) [Andrews et al. \(2010\)](#), (11) [Sylvester et al. \(1996\)](#), (12) [Stern et al. \(1994\)](#).

4. RESULTS

4.1. VLA Images

We created synthesized VLA Ka band (34 GHz, 8.8 mm) and C band (6 GHz, 5 cm) images of the HD 98800 system using a Briggs weighting (robust parameter=0.5), yielding 1σ rms= $10 \mu\text{Jy beam}^{-1}$, beam = $0.12 \text{ arcsec} \times 0.06 \text{ arcsec}$ and a beam with a position angle (PA) = 79° . A natural-weighted image (1σ rms = $9 \mu\text{Jy beam}^{-1}$, beam = $0.14 \text{ arcsec} \times 0.08 \text{ arcsec}$, PA = 78°) was also produced to derive more reliable fluxes. The 8.8 mm images clearly resolve the disk around HD 98800 B and its inner cavity for the first time, revealing a disk structure suggestive of a limb-brightened ring with a diameter of $\approx 0.1 \text{ arcsec}$. The A component is also detected at 8.8 mm as an unresolved source. At the C band, only the Briggs-weighted image (robust parameter = 0.5, 1σ rms = $15 \mu\text{Jy beam}^{-1}$, beam = $0.69 \text{ arcsec} \times 0.28 \text{ arcsec}$, PA = 23°) separates both components, but the disk is not resolved at this longer wavelength. Despite not having a known disk around it, HD 98800 A is brighter than HD 98800 B at 5 cm.

Figure 1 shows the Briggs-weighted Ka band and C band images, and an overlay of both. For comparison, we have applied a correction to the C band images to account for the measured proper motion of the HD 98800 system ($\mu_\alpha \cos(\delta) = 85.4 \text{ mas yr}^{-1}$, $\mu_\delta = 33.1 \text{ mas yr}^{-1}$, [van Leeuwen 2007](#)).

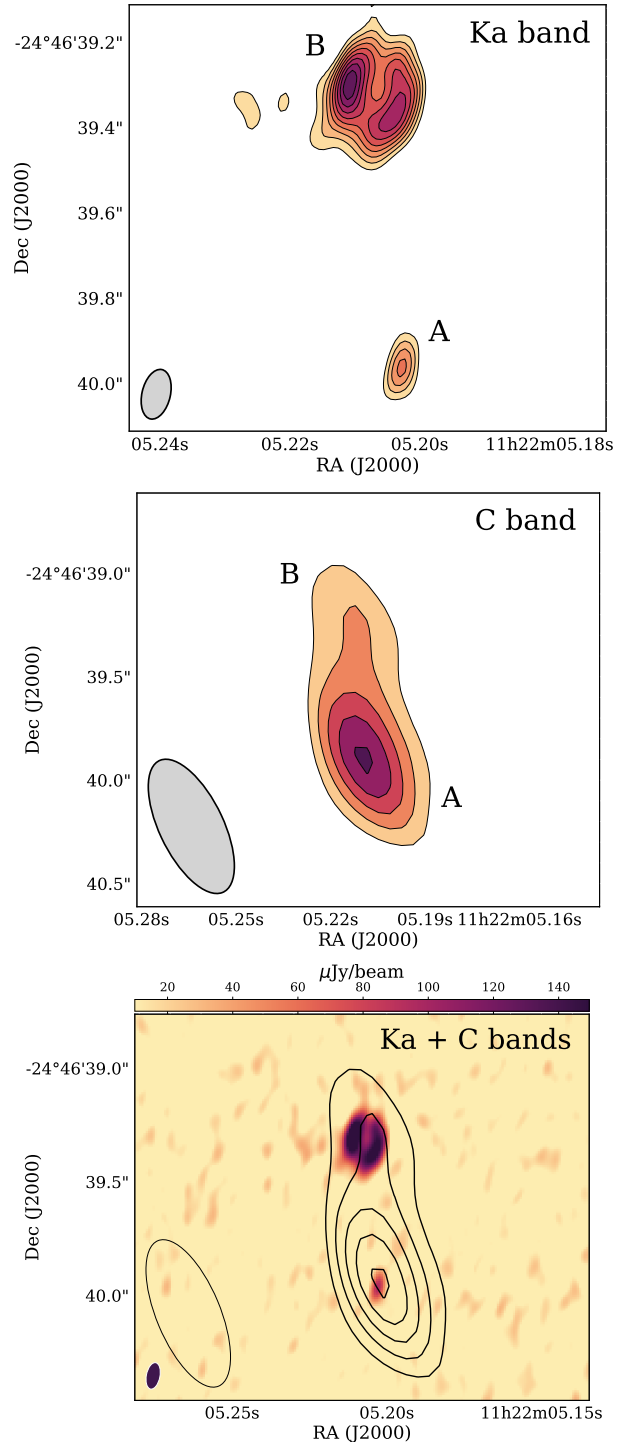


Figure 1. VLA observations of the HD 98800 system. Top: Ka band (8.8 mm) Briggs-weighted image (1σ rms= $10 \mu\text{Jy beam}^{-1}$, beam= $0.12 \text{ arcsec} \times 0.06$). Middle: C band (5 cm) Briggs-weighted image (1σ rms= $15 \mu\text{Jy beam}^{-1}$, beam= $0.69 \text{ arcsec} \times 0.28 \text{ arcsec}$). In both cases, contours start at 3σ and increase in 2σ -steps. The corresponding beams are shown as gray ellipses. Bottom: Ka band image with overlaid contours from the C band, for comparison. The C band images have been corrected from proper motion. The corresponding beams are shown in the bottom left corner (filled ellipse for the Ka band, empty ellipse for the C band).

4.2. VLA fluxes

We used the natural-weighted image at Ka band to derive fluxes both for HD 98800 A and B, since the components are well separated. Their fluxes were estimated by repeatedly measuring them in different regions placed around each source. This yielded fluxes of $70 \pm 10 \mu\text{Jy}$ for A and of $810 \pm 90 \mu\text{Jy}$ for B. Since the A component is unresolved, we also fitted a 2D Gaussian to it using the Common Astronomy Software Applications package (CASA, McMullin et al. 2007), and derived a total integrated flux of $80 \pm 10 \mu\text{Jy}$ and a peak flux of $90 \pm 10 \mu\text{Jy}$ (the resulting fit confirmed that A is unresolved). We adopted a final value for the flux of HD 98800 A of $80 \pm 15 \mu\text{Jy}$ at 34 GHz.

At the C band, natural weighting barely separates the two components, and thus we used Briggs weighting to estimate their 5 cm fluxes. In this case, the flux of each source was calculated by fitting two Gaussians to the observed emission using the task *imfit* in CASA, yielding integrated and peak fluxes of $160 \pm 30 \mu\text{Jy}$ and $170 \pm 20 \mu\text{Jy}$ for A, and $100 \pm 30 \mu\text{Jy}$ and $75 \pm 15 \mu\text{Jy}$ for B, respectively. Therefore, we assigned a final 6 GHz flux of $160 \pm 30 \mu\text{Jy}$ to HD 98800 A and $90 \pm 30 \mu\text{Jy}$ to HD 98800 B.

Circular polarization was also searched for using the VLA observations. We processed the right and left polarization images both at Ka and C bands using the Briggs-weighted images. At the Ka band, the polarization fluxes were determined to be $100 \pm 25 \mu\text{Jy}$ (right) and $90 \pm 25 \mu\text{Jy}$ (left) for A and $790 \pm 50 \mu\text{Jy}$ (right) and $770 \pm 70 \mu\text{Jy}$ (left) for B. In both polarizations, the disk around HD 98800 B is resolved, with no hint of emission from a central source. At C band, the corresponding fluxes are $200 \pm 30 \mu\text{Jy}$ (right) and $140 \pm 20 \mu\text{Jy}$ (left) for A, and $80 \pm 20 \mu\text{Jy}$ (right) and $70 \pm 20 \mu\text{Jy}$ for B. Thus, only the 5 cm emission of HD 98800 A shows signatures of some polarization in the VLA data, which could indicate the presence of nonthermal gyrosynchrotron emission.

In all cases, the reported uncertainties include the 10% systematic VLA flux calibration uncertainty.

The complete SEDs of HD 98800 A and B, including the new VLA fluxes, are shown in Figure 2.

4.3. Spectral indices

The millimeter spectral index α of the disk emission ($F_\nu \propto \nu^\alpha$) is informative of some of its properties. If the emission is optically thin, α traces the maximum size of dust grains, with $\alpha > 3$ indicating small sizes (e.g., interstellar medium (ISM)-like grains have $\alpha = 3.6 - 3.8$), while values closer to $\alpha = 2$ suggest grain growth to mm/cm sizes (Natta et al. 2004; Ricci et al. 2010a,b; Ribas et al. 2017). On the other hand, optically

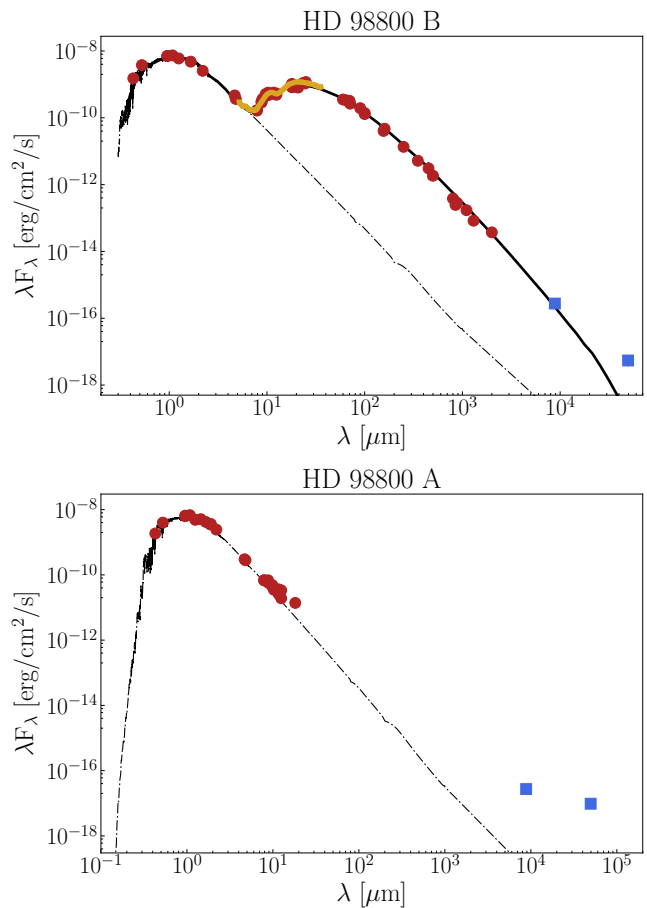


Figure 2. SEDs of HD 98800 B (top) and HD 98800 A (bottom). Ancillary (red dots) and VLA (blue squares) photometry are shown. Uncertainties are smaller than the symbol sizes. The *Spitzer*/IRS spectrum of HD 98800 B (orange line) is also shown. Dashed lines are the corresponding stellar photospheres. In the case of HD 98800 B, the best-fitting disk model is plotted as a solid black line. The adopted model reproduces the shape of the SED (in particular, its spectral index) up to the VLA Ka-band observations (8.8 mm). The C-band (5 cm) VLA flux is significantly above the photospheric emission and is too shallow to originate from dust thermal emission, suggesting that an additional emission mechanism becomes important at longer wavelength. In the case of A, the tentative excess at $18 \mu\text{m}$ like originates from uncertainties in separating the contribution of each component in unresolved photometry (see Prato et al. 2001).

thick emission will also display $\alpha = 2$, corresponding to blackbody radiation.

We estimated the millimeter spectral index α of the disk around HD 98800 B by fitting a power law to the observed fluxes in the logarithmic scale ($\log F_\lambda = -\alpha \log \lambda + C$) using the implementation of the Affine Invariant Markov Chain Monte Carlo (MCMC) (Goodman & Weare 2010) in the *emcee* (Foreman-Mackey et al. 2013) Python package. Uniform priors were adopted for both parameters (α and C). The minimum photometric uncertainty was set to 10% to avoid excessive weighting of individual data. The spectral index be-

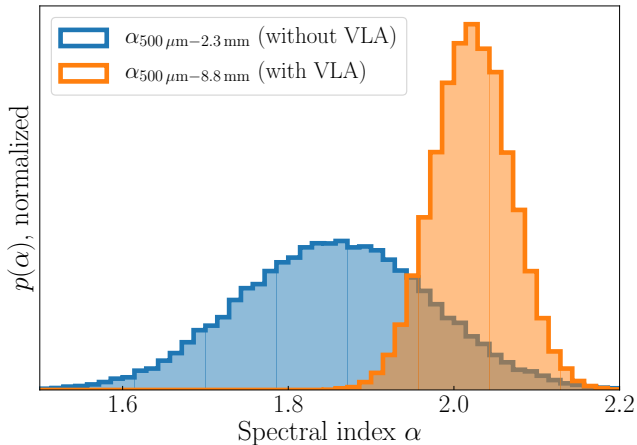


Figure 3. Posterior distributions for the millimeter spectral index α , derived between $500 \mu\text{m}$ and 2.3 mm (without VLA data, blue) and between $500 \mu\text{m}$ and 8.8 mm (with VLA data, orange).

tween $500 \mu\text{m}$ and 2.3 mm (without including the new VLA data) is $\alpha = 1.9^{+0.2}_{-0.1}$ and becomes $\alpha = 2.02^{+0.1}_{-0.05}$ when the VLA flux at 8.8 mm is included, which is consistent with either optically thick emission or optically thin emission from large grains (quoted values and uncertainties correspond to the median and the 16- and 84-percentiles, respectively). The obtained posterior distributions are shown in Figure 3. The results do not change significantly if a different wavelength range is used (e.g., $\alpha = 2.09^{+0.14}_{-0.07}$ from 1 to 8.8 mm).

We did not include the C band VLA flux in the estimate of the spectral index of HD 98800 B; for wavelengths longer than $5\text{--}7 \text{ mm}$, additional contribution from mechanisms other than thermal dust emission, such as free-free emission from photoevaporative disk winds or gyrosynchrotron radiation from stellar activity, can become significant (Pascucci et al. 2012; MacGregor et al. 2015; Macías et al. 2016; Booth et al. 2017). Indeed, the spectral index between the VLA Ka and C bands is $\alpha = 1.3^{+0.4}_{-0.2}$, showing that there is contribution from (at least) one of these processes. In the case of a photoevaporative wind, unpolarized emission with a spectral index of $-0.1 > \alpha > 0.6$ is expected, whereas gyrosynchrotron radiation is highly variable, can appear polarized, and has a negative α value. Due to the lack of observations between 8.8 mm and 5 cm , it is not possible to determine the wavelength at which the break in the spectral index occurs, and thus we cannot distinguish between these explanations. However, given the non-detection of polarization, the presence of gas in the system and the proposed evolutionary scenario, it is likely that photoevaporation is taking place in the disk. In that case, it is also possible that the 8.8 mm flux has some contribution from free-free emission. If this contribution is important, the resolved VLA images may be partially

tracing the photoevaporative wind, making HD 98800 B a great source for studying the photoevaporation of protoplanetary disks. Follow-up observations that improve the wavelength coverage at millimeter wavelengths will be able to quantify the relevance (if any) of free-free emission at 8.8 mm and test this idea in further detail.

In contrast with HD 98800 B, the A component shows no infrared excess and it is thought to be diskless (e.g. Koerner et al. 2000; Prato et al. 2001). However, both the Ka and C band VLA fluxes are clearly above the expected photospheric level and the spectral index between these two bands is $\alpha = -0.40^{+0.30}_{-0.15}$, which, together with the partial polarization measured at 5 cm , suggests that either free-free emission from a previously unknown disk or chromospheric activity (or both) are present in HD 98800 A.

4.4. A disk model of HD 98800 B

While general estimates of the disk structure can be obtained directly from the resolved images, the elongation of the beam makes it difficult to draw more precise values for some morphological parameters. We therefore used a disk model to estimate some of its properties by simulating the VLA observations. Our aim was to determine the disk spatial parameters (i.e., inner and outer radii, inclination, and PA) while reproducing the overall shape of the SED. We did not attempt to fit the dust mineralogy; for studies of the dust composition in HD 98800 B, see Furlan et al. (2007) and Olofsson et al. (2012).

We used the radiative transfer code MCFOST (Pinte et al. 2006) to produce the disk model. The distance was assumed to be 45 pc (van Leeuwen 2007; Donaldson et al. 2016). We set up two stars to account for the two components of HD 98800 B; component Ba with $T_* = 4200 \text{ K}$, $R_* = 1.1 R_\odot$, $M_* = 0.7 M_\odot$; and Bb with $T_* = 4000 \text{ K}$, $R_* = 0.9 R_\odot$, $M_* = 0.6 M_\odot$, separated by a distance of 1 au (Boden et al. 2005). As a starting point, we made crude estimates of some disk parameters from the image, setting the disk inner and outer radii to 3 and 5 au , respectively, the inclination to $\approx 45 \text{ deg}$, and the PA to $\approx 0 \text{ deg}$. The dust grain size distribution was assumed to follow $n(a) \propto a^{-p} da$, where a is the grain size, and we set $p = 3$ based on the results of Olofsson et al. (2012). We adopted an astronomical silicates composition for the dust (Draine & Lee 1984). The observed spectral index $\alpha = 2$ required a significant amount of mass of large particles, and we obtained a good overall SED fit with a dust mass of $5 \times 10^{-5} M_\odot$ and minimum and maximum dust grain sizes from $1 \mu\text{m}$ to 1 cm . The minimum grain size in protoplanetary disks is usually assumed to be much smaller, $a \approx 0.005 \mu\text{m}$, as in the ISM. However, given the age of the system, significant dust growth is expected in the disk and is in

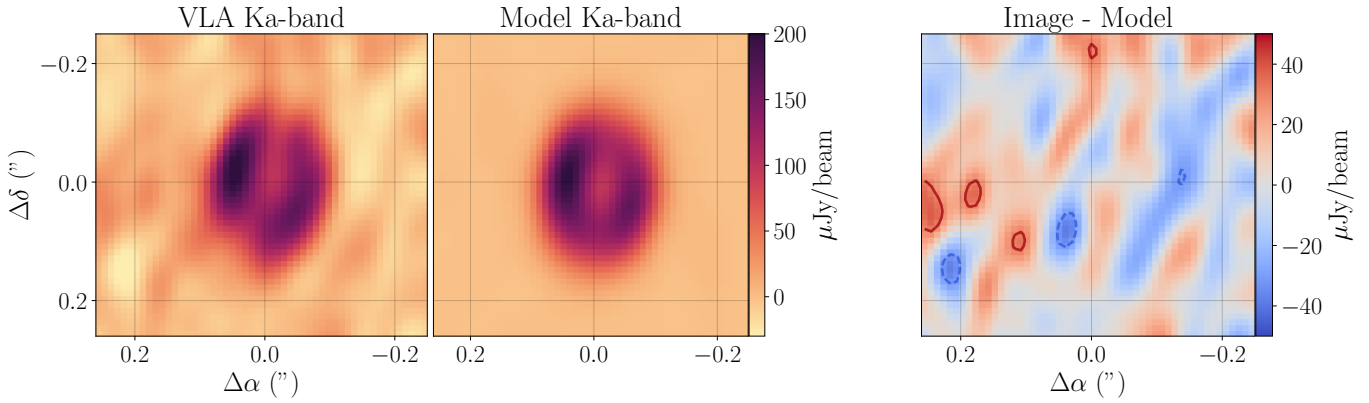


Figure 4. VLA Ka-band observation (left) of the disk around HD 98800 B , and best-fit simulated image (middle). The color scale ranges from -3σ to 20σ . Right: residuals of the best-fit model. Positive values are shown in red, negative are shown in blue. Dashed blue and red solid contours show structures below and above -3σ and 3σ , respectively. In this case, the color scale ranges from -5σ to 5σ .

agreement with the aforementioned broad silicate feature. Expanding the grain size distribution to smaller sizes does not affect the shape of the millimeter emission significantly, but much more mass is required to account for the observed flux levels. The surface density profile used follows $\Sigma(r) \propto r^{-1}$. We then changed the scale height of the disk so that it matched the shape of the observed SED, affecting mostly the mid- and far-IR emission: adopting a flaring law $h(r) = h_0(r/10 \text{ au})^{1.1}$, $h_0=0.6 \text{ au}$ at 10 au produced the best results. We note that this value probably does not represent the vertical structure of the disk accurately because our models do not include dust settling (e.g., Dullemond & Dominik 2004), which concentrates large grains in the midplane. Given the additional complexity of this process, we chose not to incorporate it in our modeling, because it will not impact the results for the spatial parameters of the disk (see below). However, a more settled midplane would also be optically thicker, and thus a settled disk with a lower mass could also produce the observed spectral index of ≈ 2 . For completeness, we also included a small ($2.5\text{-}2.6 \text{ au}$), optically thin ring with $8 \times 10^{-3} M_{\text{Moon}}$ of small dust ($0.25\text{-}1 \mu\text{m}$) to reproduce the overall shape of the IRS spectrum, although this component is not relevant for the mm-cm emission of the system.

Given the complex structure of the multiple system, we do not aim at fitting the VLA visibilities. Instead, we used MCFOST and the parameters used in the SED model to produce a grid of 625 disk images by varying the inner and outer radii (R_{in} and R_{out}), inclination (i), and PA of the disk. Five different values were tried for each parameter: R_{in} from 2.5 au to 3.5 au in steps of 0.25 au , R_{out} from 5 au to 6 au in steps of 0.25 au , i from 30° to 50° in steps of 5° , and PA from -20° to 20° in steps of 10° . These ranges were chosen based on visual inspection of the VLA image. We Fourier transformed the synthetic model images using the same uv cover-

age as the observations to obtain the simulated visibilities. Then, we obtained cleaned model images using the CLEAN task in CASA. Since our SED models do not exactly reproduce the VLA flux at 8.8 mm , we rescaled the simulated images to the measured flux in the VLA 8.8 mm Briggs-weighted image. The residuals for each image were computed, and the resulting best fit is shown in Figure 4. We used the best 10 models to derive parameter ranges from our fitting procedure. This process yielded $R_{\text{in}} = 2.75\text{-}3.25 \text{ au}$ (in agreement with the SED modeling results of Akeson et al. 2007; Andrews et al. 2010), $R_{\text{out}} = 5\text{-}5.5 \text{ au}$, $i = 40^\circ\text{-}45^\circ$, and $\text{PA} = 0^\circ - 10^\circ$. We note that there is a small -3σ residual in the south-east part of the disk. Although this might indicate a deficit of emission at that position in the disk, the spatial resolution and sensitivity of the observations do not allow us to draw any conclusion on its origin, and we do not discuss it here. Future high spatial-resolution observations will probe finer details of the disk structure and reveal if the structure is real.

The derived disk outer radius ($5 - 5.5 \text{ au}$) is smaller than the disk size of $10\text{-}15 \text{ au}$ obtained by Andrews et al. (2010) using SMA observations at $880 \mu\text{m}$. Large dust grains in protoplanetary disks are subject to radial migration due to the drag force exerted by the gas (Adachi et al. 1976; Weidenschilling 1977; Takeuchi & Lin 2002), a process that concentrates large grains in the inner regions of the system and results in wavelength-dependent disk sizes. This effect has already been observed in several cases (e.g. Guilloteau et al. 2011; Pérez et al. 2015; Tazzari et al. 2016), with disks appearing smaller at longer wavelengths. While it is possible that radial migration is the origin of the different disk-size estimates at $880 \mu\text{m}$ (SMA) and 8.8 mm (VLA) observations, we note that the SMA resolution was significantly lower (with a beam size of $0.92 \text{ arcsec} \times 0.68 \text{ arcsec}$) and the disk was only marginally resolved. Additionally, the PA

from SMA observations (160°) is also different than the one suggested by the VLA observations ($0^\circ - 10^\circ$). We thus consider that the most probable explanation for the difference in disk size is that the resolution of the SMA observations was not sufficient to derive an accurate disk radius, although radial migration cannot be ruled out. Observations at (sub)mm wavelengths with higher angular resolution will provide more accurate disk-size estimates at shorter wavelengths and will confirm dust radial migration in HD 98800 B, if present.

5. DISCUSSION

5.1. HD 98800 B: likely a protoplanetary disk

The nature of HD 98800 B is uncertain given its properties and the current understanding of disk evolution. It has usually been considered as a young, peculiar debris disk (e.g. Verrier & Evans 2008; Olofsson et al. 2012) based on its age (≈ 10 Myr, Webb et al. 1999; Weinberger et al. 2013) and the fact that it is well fit with a single blackbody (e.g. Furlan et al. 2007; Kennedy & Wyatt 2013). However, some of its properties do not match those of debris disks, which has typically been interpreted as a result of HD 98800 B being an intermediate stage between a protoplanetary and a debris disk. The presented VLA observations provide additional information about the source:

1. The fractional luminosity, f , of a disk is defined as the total luminosity of the disk with respect to that of the central object. For HD 98800 B, f is found to be $\approx 20\%$ based on our SED model, which is in agreement with previous works (10–20%, Furlan et al. 2007; Kennedy & Wyatt 2013). In contrast, debris disks display much lower fractional luminosities, typically $f \lesssim 1\%$ (e.g. Wyatt 2008; Matthews et al. 2014; Hughes et al. 2018).
2. A fractional luminosity of 20% requires that the solid angle of the disk, as seen from the star, is large. This needs a large opening angle/flaring which, in turn, favors the idea that the structure of the disk is dominated by gas. While an increasing number of debris disks have been found to harbor gas (e.g. Moór et al. 2017; Péricaud et al. 2017), their content is much lower than those of protoplanetary ones.
3. Such a high fractional luminosity also requires that the dust is mostly optically thick at optical/near-IR wavelengths, where the bulk of stellar radiation is emitted – otherwise, even with a large solid angle, the disk emission would be weaker. In contrast, debris disks are optically thin at all wavelengths (Hughes et al. 2018).
4. The detection of [OI] (Riviere-Marichalar et al. 2013, 2016) and H_2 (Yang et al. 2012) directly confirms the presence of gas content in the disk. In particular, H_2 has not been found in any debris disk so far because it is not expected to arise from planetesimal collisions and will, therefore, trace primordial gas.
5. The spectral index of HD 98800 B is $\alpha = 2$ up to 8.8 mm. Such a spectral index could indicate either optically thick emission or an optically thin disk with a gray opacity law in the millimeter. However, most debris disks show spectral indices of $\alpha = 2.5 - 3$ (Holland et al. 2017; Sibthorpe et al. 2018), which are inconsistent with the one observed in this source. Together with the other features, this suggests that the disk emission is, in fact, optically thick at millimeter wavelengths.

The combination of these pieces of evidence suggests that the disk around HD 98800 B is probably not a debris disk, but instead may be a massive (optically thick) and gas-rich *ring*; a result of the gravitational interactions of both the Ba+Ba pair and the A companion. Using the typical gas-to-dust mass ratio of 100 in protoplanetary disks, our combined SED+image modeling yields a disk mass of $5 M_{\text{Jup}}$ (albeit largely uncertain, because the dust mass could be both higher due to the emission being optically thick and lower if settling is included in the modeling). This disk would have a high density, and planet formation may thus still be possible in the system. Additionally, such a compact, optically thick ring would also explain the lack of CO detection by previous studies (Zuckerman et al. 1995; Andrews et al. 2010), given its small surface area. Follow-up observations of this target with the Atacama Large Millimeter/submillimeter Array (ALMA) will search for CO in the disk with higher sensitivity levels, testing this hypothesis.

5.2. Implications for disk evolution in HD 98800

Given the 10 Myr age of HD 98800 B, it is surprising that the system still retains a massive disk. Most protoplanetary disks around single stars disperse within that timescale, but binary and multiple systems have complex dynamical interactions that can disperse their disks much faster (e.g. Cieza et al. 2009; Harris et al. 2012; Kraus et al. 2012). Recently, Rosotti & Clarke (2018) have shown that the presence of a close companion ($a < 20\text{--}30$ au) can even alter the normal evolution of the disk from the standard inside-out dispersal (as in single stars) to an outside-in evolution, also resulting in reduced lifetimes. However, multiplicity may also be the key to explain the long-lived disk around HD 98800 B.

A number of papers have studied the dynamics of the system as a debris disk. [Akeson et al. \(2007\)](#) modeled it as a triple system (Ba-Bb-A) by distributing test particles from 2 to 15 au around the B pair, and the resulting disk extended from 3 to 10 au (and also showed substantial warping due to the effect of A). The modeling of [Verrier & Evans \(2008\)](#) suggested three different structures (a prograde coplanar disk, a second retrograde disk, and a surrounding halo) extending from 4 to 15 au. Interestingly, the VLA images show a quite symmetric, featureless disk, although future observations with higher resolution may reveal smaller structures. Later, numerical simulations by [Domingos et al. \(2012\)](#) predicted outer disk radii ranging from 7.8 to 12.2 au, depending on the orbital parameters used. While of great interest for the study of particle dynamics in multiple systems, we note that all of these works derived outer radii larger than the value obtained from the resolved VLA 8.8 mm image. A feasible explanation for this is that none of these studies included gas in their simulations, leading to a different disk behavior and evolution.

Companions can play a major role in the evolution of a gas-rich disk through tidal forces, both from the circumprimary (a disk surrounding one of the components) and circumbinary (a disk surrounding both stars) points of view.

1. Binaries surrounded by a circumbinary disk transfer angular momentum to the material in the inner regions of the disk through tidal torques, accelerating this material and stopping its inward motion; this process truncates the inner disk and opens up a gap. As an example, [Artymowicz & Lubow \(1994\)](#) found that, for a reduced mass of $\mu=0.3$, the disk is truncated at $2a-2.5a$ (where a is the semi-major axis of the binary) for eccentricities $e=0$ and 0.4 , respectively. Considering that the truncation radius increases for higher eccentricities and the orbital parameters of HD 98800 B ($a_{Ba-Bb} = 0.5$ au, $\mu = 0.45$ and $e \sim 0.8$, [Boden et al. 2005](#)), a cavity of $\sim 3-3.5$ au is not surprising for this system. [Pichardo et al. \(2008\)](#) modeled HD 98800 B using the same orbital parameters while including the effect of gas and predicted a ~ 3 au gap in the disk that is in total agreement with the presented observations. The effect of the inner binary also reduces the accretion rate onto the central sources drastically (or completely), resulting in longer-lived disks around close binaries with respect to single stars ([Alexander 2012](#)).
2. On the other hand, the torque exerted by the external companion of a circumprimary disk removes angular momentum from its outer regions,

hence slowing (or completely stopping) its viscous diffusion; circumprimary disks have truncated outer radii. [Artymowicz & Lubow \(1994\)](#) derived disk truncation radii of $0.2a-0.3a$ for a reduced mass, $\mu = 0.3$ and an eccentricity, $e = 0.4$, and this truncation radius decreases with increasing μ . If we now consider the A and B components and adopt $M_A = 1.1 M_\odot$ ([Tokovinin 1999](#)), $M_B = M_{Ba} + M_{Bb} = 1.3 M_\odot$ ([Boden et al. 2005](#)), $a_{A-B} = 45$ au, and $e = 0.4$ ([Tokovinin et al. 2014](#)), the truncation radius of the outer disk is $\lesssim 10$ au. Modeling efforts by [Pichardo et al. \(2005\)](#) found that, for a system with $\mu \approx 0.5$, the maximum value for the outer radius of the disk is 10% of the semi-major axis, or ~ 5 au (when using the updated semi-major axis of $a = 1.03$ arcsec in [Tokovinin et al. 2014](#)). Once again, this value is in perfect agreement with the VLA observations.

Since the material in the disk cannot freely accrete onto the central sources or diffuse to larger radii, its viscous evolution is considerably slowed down or stopped completely. Yet, the extreme ultraviolet and X-ray emission from the Ba-Bb pair can still produce mass loss via photoevaporative winds ([Font et al. 2004](#); [Owen et al. 2011](#)). In particular, [Kastner et al. \(2004\)](#) determined an X-ray luminosity value of $L_X = 1.4 \times 10^{29}$ erg s $^{-1}$ for HD 98800 B, which implies a mass-loss rate due to photoevaporation of $5 \times 10^{-10} M_\odot \text{ yr}^{-1}$ using the disk wind prescription in [Owen et al. \(2011\)](#). As pointed out in [Alexander \(2012\)](#), such a mass loss appears to be incompatible with the $3 \times 10^{-4} M_\odot$ disk mass estimate in [Andrews et al. \(2010\)](#), because the resulting disk lifetime (~ 0.5 Myr) is much shorter than the 10 Myr age of the TW Hya association. However, the presented VLA observations offer two solutions to this problem by suggesting both a much higher mass value ($> 5 M_{Jup}$ in our MCFOST model) and a very small disk. The new mass yields an updated disk lifetime of > 10 Myr by itself and a smaller disk size would decrease the mass-loss rate with respect to a full disk given its smaller surface area, hence bringing the expected photoevaporative rate to agreement with the age of the system.

All these results imply that the disk around HD 98800 B may have evolved considerably slower than those around single stars due to the truncation of both its inner and outer radii. This truncation produces an important (or total) suppression of accretion onto Ba-Bb (explaining the lack of accretion signatures, [Soderblom et al. 1996](#); [Muzerolle et al. 2000](#)), and thus most of the mass remains locked in the disk and is subject to evolution via photoevaporative winds. This scenario successfully explains the presence of a massive, gas-rich disk in a 10 Myr old multiple system, the apparent lack of ac-

cretion, as well as possible free-free emission from this wind that could produce the much flatter spectral index of the SED between the 8.8 mm and 5 cm VLA fluxes.

Given that HD 98800 is a bound system, it is very likely that all of its components are coeval. Moreover, the masses of A and B are somewhat comparable; Tokovinin (1999) proposed that they have the same stellar mass, and Prato et al. (2001) found values of 1.1 and $1.6 M_{\odot}$ for A and B, respectively. Therefore, the presence of a massive disk around HD 98800 B and the diskless HD 98800 A (see also Sec. 5.3 below) are challenging if we assume that both formed with a disk (e.g., Prato et al. 2001). The evolutionary scenario proposed earlier (i.e., the accretion rate is strongly suppressed in HD 98800 B by Ba-Bb, and the disk is evolving through photoevaporative winds only) offers an explanation to this issue. HD 98800 A is itself a binary (Aa-Ab), so it is possible that accretion was also suppressed in it. However, Kastner et al. (2004) found its X-ray luminosity to be ≈ 4 times higher than in HD 98800 B. Assuming that this ratio has been constant throughout the lifetime of the system, it implies a mass loss through photoevaporative winds about ≈ 5 times higher for A ($\dot{M}_{\text{wind}} \propto L_X^{1.14}$, Owen et al. 2011), and thus its dispersal would have been significantly faster. The mass of the disk is also known to scale linearly with stellar mass (although with significant scatter, Andrews et al. 2013; Pascucci et al. 2016), and the results of Prato et al. (2001) then suggest that the disk around A was probably less massive. These two facts combined could explain why HD 98800 A is already diskless.

Interestingly, the TW Hya association contains another long-lived disk in a multiple system with several features resembling those of HD 98800: TWA 3, a hierarchical triple system that comprises a close binary (Aa-Ab, e.g. Muzerolle et al. 2000) surrounded by a circumbinary disk and orbited by a visual companion at 40-110 au (de la Reza et al. 1989; Reipurth & Zinnecker 1993; Webb et al. 1999; Torres et al. 2003; Kellogg et al. 2017). The small binary separation and eccentricity ($a=0.2$ au, $e=0.6$, Kellogg et al. 2017) explain the 1 au cavity inferred from SED modeling (Andrews et al. 2010). Such a small cavity may allow some mass accretion via streams, accounting for its low accretion rates (5×10^{-11} - $2.5 \times 10^{-10} M_{\odot} \text{ yr}^{-1}$, Muzerolle et al. 2000; Herczeg et al. 2009) and its observed periodicity, similar to the binary period (Tofflemire et al. 2017). As discussed in Kellogg et al. (2017), this system is also interesting from an evolutionary perspective, since the B component is diskless. The evolutionary scenario proposed here for HD 98800 also works for TWA 3: while the disk around TWA 3B likely evolved on regular timescales through viscous evolution and photoevaporation, the mass-accretion rate of the TWA 3A is signifi-

cantly reduced by the Aa-Ab pair, resulting in a longer disk lifetime. Their ages, comparable disk properties, and system architectures suggest that both HD 98800 B and TWA 3 could have survived through the same mechanisms, and comparative studies of these two systems offer a great opportunity for understanding the importance of star-disk interactions and multiplicity in disk evolution.

Although the proposed scenario provides plausible explanations for several properties of the disk around HD 98800 B, it also presents an issue: the simulations of Artymowicz & Lubow (1996) predict that, despite the cavity formed in circumbinary disks by the binary system, some material can still accrete onto the central sources through gas streams. In the case of eccentric systems, this accretion would be periodic, with a period similar to that of the binary. This phenomenon has been found in other circumbinary disks, such as DQ Tau (Mathieu et al. 1997), UZ Tau E (Jensen et al. 2007), and TWA 3A (Tofflemire et al. 2017), which raises the question of why HD 98800 B does not show a similar behavior. Although we do not have a clear explanation for this, a number of scenarios could account for the apparent lack of periodic accretion in HD 98800 B. A likely possibility is that periodic accretion actually exists in the system, but at a very low rate that makes its detection challenging; in fact, Yang et al. (2012) suggest that HD 98800 B is an accreting source. The authors note that previous studies were unable to find accretion signatures in the system, and their low-resolution optical spectrum places an upper limit of $10^{-9.9} M_{\odot} \text{ yr}^{-1}$ to its accretion rate. However, their detection of H_2 suggests ongoing accretion at lower rates given that H_2 is not detected in nonaccreting systems (Ingleby et al. 2009) but can still be seen in very slow accretors (Ingleby et al. 2011). It is even possible that the periodic nature of accretion in the system is responsible for some of the previous nondetections of accretion signatures. A second explanation could be that HD 98800 B displays more extreme orbital parameters, because the three systems mentioned above have all shorter periods (and hence smaller separations) and lower eccentricities: for comparison, DQ Tau shows $P=15.8$ days and $e=0.56$ (Czekala et al. 2016), UZ Tau E has $P=19.2$ days and $e=0.33$ (Jensen et al. 2007), and TWA 3A has $P=34.9$ days and $e=0.63$ (Kellogg et al. 2017), in contrast with the $P=315$ days and $e=0.78$ of HD 98800 B. It is thus possible that, under these different orbital conditions, gas streams cannot form or are less efficient. Moreover, the significantly longer period of HD 98800 B makes it harder to study any periodic variability. Long-term monitoring with high sensitivity is required to confirm the low mass-accretion rate of HD 98800 B and to identify any possible variability in it.

5.3. The emission from HD 98800 A

HD 98800 A is detected at both 8.8 mm and 5 cm in the synthesized VLA images and becomes brighter than B in the latter wavelength. The flux detected in both cases is well above the expected photospheric level (see Figure 2), indicating additional contribution from other mechanisms. One possible explanation for this excess is the presence of a previously unknown circumstellar disk around A. However, the emission is unresolved at 8.8 mm, meaning that the corresponding disk radius would have to be < 2.5 au, smaller than the expected truncation radius due to the B (e.g., [Papaloizou & Pringle 1977](#); [Artymowicz & Lubow 1994](#)). The dust in such a disk would be very close to the central stars and would thus emit significantly in the infrared. However, no infrared excess has been found in HD 98800 A (e.g. [Koerner et al. 2000](#); [Prato et al. 2001](#)). Given the negative spectral index of the emission and the partial polarization detected at 5 cm, stellar activity appears as a better explanation the observations, as proposed by [Kastner et al. \(2004\)](#) in the light of *Chandra* X-ray observations of HD 98800; the A component was found to be ~ 4 times brighter than B, and a flaring event was even detected during the observations, suggesting that the star is significantly active. Higher-resolution observations with ALMA will probe smaller scales and confirm or deny the presence of a small disk around HD 98800 A, clarifying the nature of the detected excess at mm/cm wavelengths.

6. SUMMARY AND CONCLUSIONS

We present Ka band (8.8 mm, 34 GHz) and C band (5 cm, 6 GHz) VLA observations of the hierarchical quadruple system HD 98800 in the 10 Myr old TW Hya association. The 8.8 mm observations successfully resolve the disk and the inner cavity around the B component and detect unresolved emission from A. Both A and B are also detected (unresolved) at 5 cm. Only the 5 cm emission from A shows signatures of polarization. We use the MCFOST radiative transfer software to model both the SED and the resolved VLA image of the disk. The main results of the study are:

1. The (sub)mm spectral index of the disk around HD 98800 B is ≈ 2 up to 8.8 mm, suggesting either optically thin radiation from a dust population with a gray opacity law at millimeter wavelengths or optically thick emission.
2. The disk extends from 3 to 5 au at 8.8 mm. The values of both the inner and outer radii (truncated by the Ba-Bb and the interaction with A, respectively) agree with model predictions of viscous disk interactions with companions.

3. For such a disk size, we were unable to reproduce the observed 8.8 mm flux and spectral index with an optically thin disk. Combined with previous detections of gas in the system, this suggests that HD 98800 B is probably a massive, optically thick and gas-rich disk, more similar to protoplanetary than to debris disks.
4. Given that both disk fractions and exoplanet occurrence are lower in close binaries than around single stars, the survival of a massive disk in a quadruple system, such as HD 98800 B, appears to contradict disk evolution theories. We suggest that the inner and outer truncation of the disk have stopped the viscous evolution of the disk, which is thus governed by photoevaporation. The small size of the disk lowers the mass-loss rate through photoevaporation, explaining the longevity of the disk. This scenario results in longer disk lifetimes that may ease planet formation in multiple systems with the appropriate configuration.
5. The spectral index of HD 98800 B between 8.8 mm and 5 cm is significantly shallower ($\alpha = 1.3$), indicating that additional contribution from free-free emission by photoevaporating material or from gyrosynchrotron emission from stellar activity is present at cm wavelengths. In case the photoevaporative wind is the correct explanation, then it is possible that the 8.8 mm flux is also partially probing this emission, making HD 98800 B an ideal target to study this phenomenon.
6. The disk size is 2-3 times smaller than the one derived by [Andrews et al. \(2010\)](#), who used partially resolved SMA observations at $880 \mu\text{m}$. While we attribute the difference to the lower angular resolution of SMA, if this size dependence with wavelength is, in fact, real, it may hint at significant dust radial migration in the system.
7. The A component appears unresolved both at 8.8 mm and 5 cm, and the observed fluxes are above the expected photospheric levels. In contrast to HD 98800 B, the spectral index between the two VLA bands is negative ($\alpha = -0.4$). Together with the partial polarization of the 5 cm emission of HD 98800 A, this favors a stellar origin for the excess instead of a previously unknown disk around this component.

Follow-up ALMA observations will be able to search for CO in the system with increased sensitivity with respect to previous studies and to measure the disk size at shorter wavelengths to test the dust radial migration

scenario in HD 98800 B. Additional VLA observations at other wavelengths will also provide a better sampling of the mm/cm range and will help to quantify the relative importance (if any) of free-free emission in the disk. Given its proximity and unique properties, HD 98800 offers a unique laboratory to study the impact of multiplicity on planet formation and disk evolution.

We thank the anonymous referee for their useful comments, which helped improving the quality of this manuscript. We thank Richard Alexander for discussion on disk evolution in binary systems and Eric Nielsen

for examining the orbit of HD 98800 including the VLA data presented here. This manuscript is based on data from the NSF's Karl G. Jansky Very Large Array (VLA). We have also used data from the *Herschel Space Observatory* (*Herschel*). *Herschel* is an ESA space observatory with science instruments provided by European-led Principal Investigator consortia and with important participation from NASA.

Software: emcee (Foreman-Mackey et al. 2013), MCFOST (Pinte et al. 2006), HIPE (v15; Ott 2010), CASA (McMullin et al. 2007), Matplotlib (Hunter 2007), SciPy (Jones et al. 2001), Numpy (Jones et al. 2001), pandas (McKinney 2010), Astropy (Astropy Collaboration et al. 2013).

REFERENCES

- Adachi, I., Hayashi, C., & Nakazawa, K. 1976, *Progress of Theoretical Physics*, 56, 1756
- Akeson, R. L., Rice, W. K. M., Boden, A. F., et al. 2007, *ApJ*, 670, 1240
- Alexander, R. 2012, *ApJL*, 757, L29
- Alexander, R., Pascucci, I., Andrews, S., Armitage, P., & Cieza, L. 2014, *Protostars and Planets VI*, 475
- Andrews, S. M., Czekala, I., Wilner, D. J., et al. 2010, *ApJ*, 710, 462
- Andrews, S. M., Rosenfeld, K. A., Kraus, A. L., & Wilner, D. J. 2013, *ApJ*, 771, 129
- Artymowicz, P., & Lubow, S. H. 1994, *ApJ*, 421, 651
- . 1996, *ApJL*, 467, L77
- Astropy Collaboration, Robitaille, T. P., Tollerud, E. J., et al. 2013, *A&A*, 558, A33
- Balog, Z., Müller, T., Nielbock, M., et al. 2014, *Experimental Astronomy*, 37, 129
- Boden, A. F., Sargent, A. I., Akeson, R. L., et al. 2005, *ApJ*, 635, 442
- Booth, M., Dent, W. R. F., Jordán, A., et al. 2017, *MNRAS*, 469, 3200
- Cieza, L. A., Padgett, D. L., Allen, L. E., et al. 2009, *ApJL*, 696, L84
- Czekala, I., Andrews, S. M., Torres, G., et al. 2016, *ApJ*, 818, 156
- de la Reza, R., Torres, C. A. O., Quast, G., Castilho, B. V., & Vieira, G. L. 1989, *ApJL*, 343, L61
- Dent, W. R. F., Greaves, J. S., & Coulson, I. M. 2005, *MNRAS*, 359, 663
- Di Francesco, J., Johnstone, D., Kirk, H., MacKenzie, T., & Ledwosinska, E. 2008, *ApJS*, 175, 277
- Domingos, R. C., Winter, O. C., & Carruba, V. 2012, *A&A*, 544, A63
- Donaldson, J. K., Weinberger, A. J., Gagné, J., et al. 2016, *ApJ*, 833, 95
- Doyle, L. R., Carter, J. A., Fabrycky, D. C., et al. 2011, *Science*, 333, 1602
- Draine, B. T., & Lee, H. M. 1984, *ApJ*, 285, 89
- Duchêne, G., & Kraus, A. 2013, *ARA&A*, 51, 269
- Ducourant, C., Teixeira, R., Galli, P. A. B., et al. 2014, *A&A*, 563, A121
- Dullemond, C. P., & Dominik, C. 2004, *A&A*, 421, 1075
- Dupuy, T. J., Kratter, K. M., Kraus, A. L., et al. 2016, *ApJ*, 817, 80
- Duquenooy, A., & Mayor, M. 1991, *A&A*, 248, 485
- Espaillet, C., Muzerolle, J., Najita, J., et al. 2014, *Protostars and Planets VI*, 497
- Font, A. S., McCarthy, I. G., Johnstone, D., & Ballantyne, D. R. 2004, *ApJ*, 607, 890
- Foreman-Mackey, D., Hogg, D. W., Lang, D., & Goodman, J. 2013, *PASP*, 125, 306
- Furlan, E., Sargent, B., Calvet, N., et al. 2007, *ApJ*, 664, 1176
- Goodman, J., & Weare, J. 2010, *Comm. App. Math. Comp. Sci.*, 5, 65
- Gregorio-Hetem, J., Lepine, J. R. D., Quast, G. R., Torres, C. A. O., & de La Reza, R. 1992, *AJ*, 103, 549
- Guilloteau, S., Dutrey, A., Piétu, V., & Boehler, Y. 2011, *A&A*, 529, A105
- Haisch, Jr., K. E., Lada, E. A., & Lada, C. J. 2001, *ApJL*, 553, L153
- Harris, R. J., Andrews, S. M., Wilner, D. J., & Kraus, A. L. 2012, *ApJ*, 751, 115
- Hartmann, L., Calvet, N., Gullbring, E., & D'Alessio, P. 1998, *ApJ*, 495, 385
- Helled, R., Bodenheimer, P., Podolak, M., et al. 2014, *Protostars and Planets VI*, 643
- Herczeg, G. J., Cruz, K. L., & Hillenbrand, L. A. 2009, *ApJ*, 696, 1589
- Hernández, J., Hartmann, L., Calvet, N., et al. 2008, *ApJ*, 686, 1195
- Hernández, J., Hartmann, L., Megeath, T., et al. 2007, *ApJ*, 662, 1067
- Holland, W. S., Matthews, B. C., Kennedy, G. M., et al. 2017, *MNRAS*, 470, 3606
- Hollenbach, D., Johnstone, D., Lizano, S., & Shu, F. 1994, *ApJ*, 428, 654
- Hughes, A. M., Duchene, G., & Matthews, B. 2018, *ArXiv e-prints*, arXiv:1802.04313
- Hunter, J. D. 2007, *Computing In Science & Engineering*, 9, 90
- Ingleby, L., Calvet, N., Bergin, E., et al. 2009, *ApJL*, 703, L137
- . 2011, *ApJ*, 743, 105
- Ishihara, D., Onaka, T., Kataza, H., et al. 2010, *A&A*, 514, A1+
- Jensen, E. L. N., Dhital, S., Stassun, K. G., et al. 2007, *AJ*, 134, 241
- Jones, E., Oliphant, T., Peterson, P., et al. 2001, *SciPy: Open source scientific tools for Python*, ,
- Kastner, J. H., Huenemoerder, D. P., Schulz, N. S., et al. 2004, *ApJL*, 605, L49
- Kellogg, K., Prato, L., Torres, G., et al. 2017, *ApJ*, 844, 168
- Kennedy, G. M., & Wyatt, M. C. 2012, *MNRAS*, 426, 91

- . 2013, *MNRAS*, 433, 2334
- Kley, W., & Nelson, R. P. 2012, *ARA&A*, 50, 211
- Koerner, D. W., Jensen, E. L. N., Cruz, K. L., Guild, T. B., & Gultekin, K. 2000, *ApJL*, 533, L37
- Kostov, V. B., Orosz, J. A., Welsh, W. F., et al. 2016, *ApJ*, 827, 86
- Kraus, A. L., Ireland, M. J., Hillenbrand, L. A., & Martinache, F. 2012, *ApJ*, 745, 19
- Kraus, A. L., Ireland, M. J., Martinache, F., & Hillenbrand, L. A. 2011, *ApJ*, 731, 8
- Kraus, A. L., Ireland, M. J., Martinache, F., & Lloyd, J. P. 2008, *ApJ*, 679, 762
- Lafrenière, D., Jayawardhana, R., Brandeker, A., Ahmic, M., & van Kerkwijk, M. H. 2008, *ApJ*, 683, 844
- Low, F. J., Hines, D. C., & Schneider, G. 1999, *ApJL*, 520, L45
- Low, F. J., Smith, P. S., Werner, M., et al. 2005, *ApJ*, 631, 1170
- Lynden-Bell, D., & Pringle, J. E. 1974, *MNRAS*, 168, 603
- MacGregor, M. A., Wilner, D. J., Andrews, S. M., Lestrade, J.-F., & Maddison, S. 2015, *ApJ*, 809, 47
- Macías, E., Anglada, G., Osorio, M., et al. 2016, *ApJ*, 829, 1
- Mamajek, E. E. 2009, in *American Institute of Physics Conference Series*, Vol. 1158, 3–10
- Mathieu, R. D., Stassun, K., Basri, G., et al. 1997, *AJ*, 113, 1841
- Mathis, J. S. 1990, *ARA&A*, 28, 37
- Matthews, B. C., Krivov, A. V., Wyatt, M. C., Bryden, G., & Eiroa, C. 2014, *Protostars and Planets VI*, 521
- McKinney, W. 2010, in *Proceedings of the 9th Python in Science Conference*, ed. S. van der Walt & J. Millman, 51 – 56
- McMullin, J. P., Waters, B., Schiebel, D., Young, W., & Golap, K. 2007, in *Astronomical Data Analysis Software and Systems XVI*, Vol. 376, 127
- Moór, A., Curé, M., Kóspál, Á., et al. 2017, *ApJ*, 849, 123
- Muzerolle, J., Calvet, N., Briceño, C., Hartmann, L., & Hillenbrand, L. 2000, *ApJL*, 535, L47
- Natta, A., Testi, L., Neri, R., Shepherd, D. S., & Wilner, D. J. 2004, *A&A*, 416, 179
- Olofsson, J., Juhász, A., Henning, T., et al. 2012, *A&A*, 542, A90
- Ott, S. 2010, in *Astronomical Society of the Pacific Conference Series*, Vol. 434, *Astronomical Data Analysis Software and Systems XIX*, ed. Y. Mizumoto, K.-I. Morita, & M. Ohishi, 139
- Owen, J. E., Ercolano, B., & Clarke, C. J. 2011, *MNRAS*, 412, 13
- Papaloizou, J., & Pringle, J. E. 1977, *MNRAS*, 181, 441
- Pascucci, I., Gorti, U., & Hollenbach, D. 2012, *ApJL*, 751, L42
- Pascucci, I., Testi, L., Herczeg, G. J., et al. 2016, *ApJ*, 831, 125
- Pearson, C., Lim, T., North, C., et al. 2014, *Experimental Astronomy*, 37, 175
- Pérez, L. M., Chandler, C. J., Isella, A., et al. 2015, *ApJ*, 813, 41
- Périck, J., Di Folco, E., Dutrey, A., Guilloteau, S., & Piétu, V. 2017, *A&A*, 600, A62
- Pichardo, B., Sparke, L. S., & Aguilar, L. A. 2005, *MNRAS*, 359, 521
- . 2008, *MNRAS*, 391, 815
- Pilbratt, G. L., Riedinger, J. R., Passvogel, T., et al. 2010, *A&A*, 518, L1
- Pinte, C., Ménard, F., Duchêne, G., & Bastien, P. 2006, *A&A*, 459, 797
- Prato, L., Ghez, A. M., Piña, R. K., et al. 2001, *ApJ*, 549, 590
- Raymond, S. N., Kokubo, E., Morbidelli, A., Morishima, R., & Walsh, K. J. 2014, *Protostars and Planets VI*, 595
- Reipurth, B., & Zinnecker, H. 1993, *A&A*, 278, 81
- Ribas, Á., Bouy, H., & Merín, B. 2015, *A&A*, 576, A52
- Ribas, Á., Espaillat, C. C., Macías, E., et al. 2017, *ApJ*, 849, 63
- Ricci, L., Testi, L., Natta, A., & Brooks, K. J. 2010a, *A&A*, 521, A66
- Ricci, L., Testi, L., Natta, A., et al. 2010b, *A&A*, 512, A15
- Riviere-Marichalar, P., Merín, B., Kamp, I., Eiroa, C., & Montesinos, B. 2016, *A&A*, 594, A59
- Riviere-Marichalar, P., Pinte, C., Barrado, D., et al. 2013, *A&A*, 555, A67
- Rosotti, G. P., & Clarke, C. J. 2018, *MNRAS*, 473, 5630
- Rucinski, S. 1993, *IAUC*, 5788
- Salyk, C., Blake, G. A., Boogert, A. C. A., & Brown, J. M. 2009, *ApJ*, 699, 330
- Shakura, N. I., & Sunyaev, R. A. 1973, *A&A*, 24, 337
- Shu, F. H., Johnstone, D., & Hollenbach, D. 1993, *Icarus*, 106, 92
- Sibthorpe, B., Kennedy, G. M., Wyatt, M. C., et al. 2018, *MNRAS*, 475, 3046
- Soderblom, D. R., Henry, T. J., Shetrone, M. D., Jones, B. F., & Saar, S. H. 1996, *ApJ*, 460, 984
- Soderblom, D. R., King, J. R., Siess, L., et al. 1998, *ApJ*, 498, 385
- Stern, S. A., Weintraub, D. A., & Festou, M. C. 1994, *IAUC*, 6003
- Sylvester, R. J., Skinner, C. J., Barlow, M. J., & Mannings, V. 1996, *MNRAS*, 279, 915
- Takeuchi, T., & Lin, D. N. C. 2002, *ApJ*, 581, 1344
- Tazzari, M., Testi, L., Ercolano, B., et al. 2016, *A&A*, 588, A53
- Testi, L., Birnstiel, T., Ricci, L., et al. 2014, *Protostars and Planets VI*, 339
- Tofflemire, B. M., Mathieu, R. D., Herczeg, G. J., Akeson, R. L., & Ciardi, D. R. 2017, *ApJL*, 842, L12
- Tokovinin, A., Mason, B. D., & Hartkopf, W. I. 2014, *AJ*, 147, 123
- Tokovinin, A. A. 1999, *Astronomy Letters*, 25, 669
- Torres, C. A. O., Quast, G. R., Melo, C. H. F., & Sterzik, M. F. 2008, *Young Nearby Loose Associations*, ed. B. Reipurth, 757
- Torres, G., Guenther, E. W., Marschall, L. A., et al. 2003, *AJ*, 125, 825
- Torres, G., Stefanik, R. P., Latham, D. W., & Mazeh, T. 1995, *ApJ*, 452, 870
- van Leeuwen, F. 2007, *A&A*, 474, 653
- Verrier, P. E., & Evans, N. W. 2008, *MNRAS*, 390, 1377
- Walker, H. J., & Wolstencroft, R. D. 1988, *PASP*, 100, 1509
- Webb, R. A., Zuckerman, B., Platais, I., et al. 1999, *ApJL*, 512, L63
- Weidenschilling, S. J. 1977, *Ap&SS*, 51, 153
- Weinberger, A. J., Anglada-Escudé, G., & Boss, A. P. 2013, *ApJ*, 762, 118
- Welsh, W. F., Orosz, J. A., Carter, J. A., et al. 2012, *Nature*, 481, 475
- Wyatt, M. C. 2008, *ARA&A*, 46, 339
- Wyatt, M. C., Smith, R., Su, K. Y. L., et al. 2007, *ApJ*, 663, 365
- Yang, H., Herczeg, G. J., Linsky, J. L., et al. 2012, *ApJ*, 744, 121
- Zuckerman, B., & Becklin, E. E. 1993, *ApJL*, 406, L25
- Zuckerman, B., Forveille, T., & Kastner, J. H. 1995, *Nature*, 373, 494